Uncertainty Determination of the Set Nikon 6B Autocollimator + Visual Interface

Guillermo J. Bergues, Clemar Schürrer, and Nancy Brambilla

***Abstract*— In this paper, we present a methodology which identifies and characterizes the sources of uncertainty associated with the operation of an electronic autocollimator. It was developed based on a commercial autocollimator—Nikon 6B model—with the addition of a visual interface and its respective image processing software. The visual interface allows the optical instrument's performance to be surpassed, thus increasing the resolution and accuracy with respect to the original equipment. The development allows for an improvement in the measurement capacity of the laboratories when calibrating electronic levels, reference planes, and angular patterns, among others. On the other hand, fundamental information is provided for the new instrument's last stage of design through a detailed evaluation of the measurement system's mathematical model. This allows us to determine the relative impact of each uncertainty component in order to identify those of greater weight and minimize them by correction.**

***Index Terms*— Autocollimator, image processing, optical distortion, uncertainty, visual interface.**

I. Introduction

DETERMINING the best measurement capacity (BMC) is an essential step in the design of measurement systems. It involves calculating the typical error contributions and then combining them with a mathematical model. In a scientific measurement, error means the inevitable uncertainty that attends all measurements. In other words, error analysis is the study and evaluation of uncertainty in measurement [1]. With the help of the instrument's mathematical model, this uncertainty can be estimated.

The estimation sought presents its difficulties because it is necessary to separately calculate each of the error contributions that appear in the measurement. However, in practice, some of them cannot be isolated from each other because the line that delimits them is diffuse or totally nonexistent [2]. In particular, this situation is present in the system defined by the set autocollimator + visual interface (A&I). In this paper, we present a method to overcome this difficulty.

In order to introduce our method, it is pertinent to recapitulate each of the previous stages of our development: in our previous work performed at the Center of Investigation and Transfer in Metrology (CEMETRO) [3], we implemented a visual interface for a Nikon 6B/6D autocollimator, whose purpose is to improve the resolution and BMC of the original instrument by giving the assembly more accuracy (see Fig. 1).

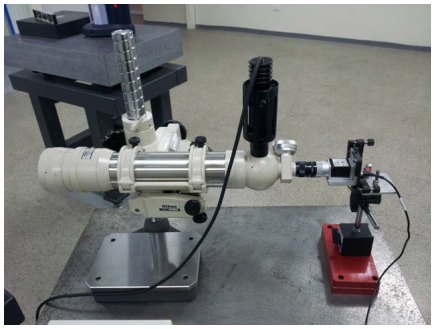

Fig. 1. Nikon 6B autocollimator with its visual interface.

In our first study [4], we showed that it was possible to make and mount an external visual interface for the autocollimator. Even though the visual interface's camera had a CMOS sensor that introduced a large field deformation, the image processing designed [5] was able to reach the resolution of the instrument. Then, we extended our first design using a high-resolution camera with a CCD sensor. This allowed us to improve the resolution and BMC of the original instrument; the results of this achievement are explained in [6]. Later, using the positional calibration of our previous work, we proceeded to improve the instrument's reticle detection algorithm with a preprocessing step aimed at reducing the optical phenomenon produced by the vignetting effect. The design process of our final algorithm is described in [7]. Measurements with the last improvement were convincing; however, there was a decrease in the capacities of A&I as the measurement was performed outside the center of the scale. This phenomenon was explained and solved in our last work [8].

With all the components of the interface in place, it was necessary to make a rigorous study of the uncertainty of A&I. Even though in [7], through a simulation, we discuss the performance of our detectors and calculate the uncertainty our software introduced in the measurement, the complete characterization of A&I and the determination of the minimum measurement uncertainty possible were lacking. Then, we proceeded to identify each contribution to the error in order to obtain the indispensable results that would complete the design process initiated in our first studies.

As a consequence of this uncertainty calculation, it was possible to determine the relative impact of each component

Manuscript received February 7, 2017; revised September 18, 2017; accepted September 28, 2017. Date of publication December 27, 2017; date of current version April 5, 2018. The Associate Editor coordinating the review process was Dr. Sebastian Catunda. *(Corresponding author: Guillermo J. Bergues.)*

The authors are with the Centro de Investigación y Transferencia en Metrología, Facultad Regional Córdoba, Universidad Tecnológica Nacional, Córdoba 4050, Argentina (e-mail: gbergues@frc.utn.edu.ar).

Color versions of one or more of the figures in this paper are available online at http://ieeexplore.ieee.org.

Digital Object Identifier 10.1109/TIM.2017.2782003

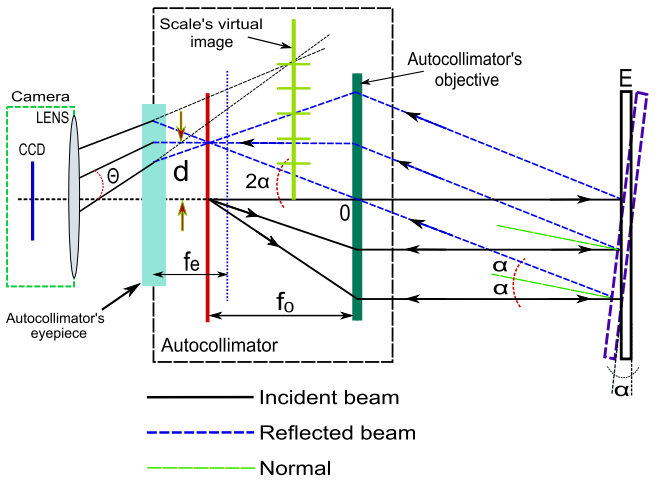

Fig. 2. A&I functioning scheme. f_0: autocollimator's focal distance, f_e: eyepiece's focal distance, d: displacement, and α: measured angle. The autocollimator reads d/f_0.

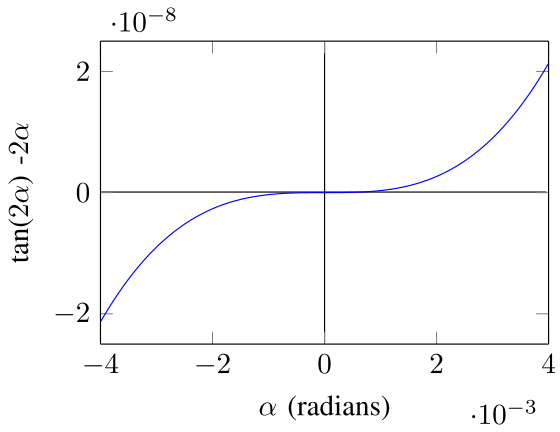

Fig. 3. Graph of the function $\tan(2\alpha) - 2\alpha$ as a function of α in the range of the autocollimator. The difference between $\tan(2\alpha)$ and 2α is very small, so we can express that $\tan(2\alpha) \approx 2\alpha$.

and identify the one of greater weight. The result allows us to determine the characteristics of the camera's objective to be chosen for the visual interface, and establishes the appropriate projection for future system improvements. On the other hand, this means a contribution for other laboratories to be able to create their own low-cost visual interfaces for their optical autocollimators.

The following sections develop the elements that add uncertainty to the measurement, while explaining the scope of work according to the state of the art (Section V). The reader can find the detailed study of temperature influence (Section III-A), the software (Section III-B), the Savitzky–Golay Filter (Section III-C), the pixels position on the CCD (Section III-D), the light source (Section III-E), the pixels matrix's orientation with respect to the cross (Section III-F), the scale's linearity and autocollimator's optics (Section III-G), beam parallelism (Section III-H), and air turbulence (Section III-I).

II. Mathematical Model of the System

The autocollimator performs the measurement according to the following relation [9]:

$$\tan(2 \cdot \alpha) = \frac{d}{f_0} \tag{1}$$

d is the reading of the scale divisions and f_0 is the autocollimator's focal distance. The autocollimator does not read α but $\tan(2\alpha)$ (see Fig. 2).

As it can be seen in Fig. 3, the difference between 2α and $\tan(2\alpha)$ is lower than two parts in 10^8 within the whole range 4.4×10^{-3}rad ($\pm 15'$). For this reason, (1) can be changed as

$$\alpha = \frac{d}{2f_0}. \tag{2}$$

A. Equation Modification When Connecting the Visual Interface

Equation (2) is based on the autocollimator's optical system; however, it cannot be applied directly once the camera is connected. There is an interaction between both the optical systems that must be taken into account [8]: the camera captures the virtual image generated by the autocollimator's optical system (see Fig. 2).

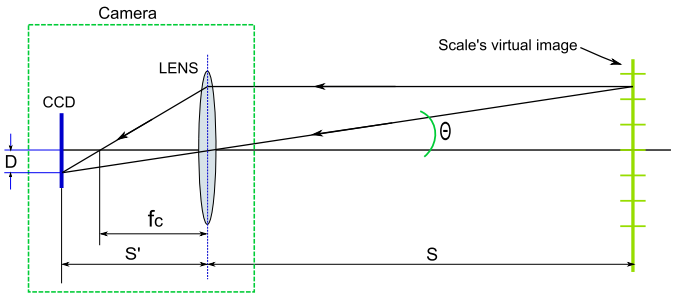

Fig. 4. Optical scheme of the camera when capturing the scale's virtual image. f_c: camera's focal distance. S': distance between the camera lens and the sensor.

First, since the angles measured with the autocollimator are very small, it is necessary to magnify them so that they can be appreciated. For this reason, the autocollimator (which behaves like a telescope from the optical point of view) has an eyepiece characterized by an eyepiece's focal distance f_e (see Fig. 2). The angular magnification M_A satisfies [10]

$$M_A = \frac{\Theta}{2\alpha} = \frac{f_0}{f_e}. \tag{3}$$

Second, if the measurement of the angle Θ is made using the camera of Fig. 2, in the paraxial approximation, the following is true:

$$\Theta = \frac{D}{S'} \tag{4}$$

where S' is the distance between the camera lens and the sensor (the image) and D is the distance measured on the CCD sensor; these distances are shown in Fig. 4. The approximation (4) can be studied in detail by means of Fig. 4, which is an enlargement of Fig. 2 in the part of the camera. By combining (3) and (4), we obtain

$$\alpha = \frac{D}{2 * S' * M_A}. \tag{5}$$

This represents the mathematical model of A&I without taking into account the thermal variations.

B. Variation of the Model With Temperature

The measured angle α undergoes a variation due to the thermal drifts in the laboratory. The variables D, S', and M_A vary according to

$$V = V_0(20\ ^\circ\text{C}) \cdot (1 + \alpha_{\text{mat}} \cdot \Delta T) \tag{6}$$

where V is any variable (D, S', and M_A) and α_{mat} is the material's coefficient of thermal expansion; e.g., the variation of D as a function of the temperature in the CCD is described by the following function: $D = D_0(20\ ^\circ\text{C}) \cdot (1 + \alpha_{Si} \cdot \Delta T)$. α_{Si} is the silicon's thermal expansion coefficient. In the same way, S' has a similar function, but α_{Steel} is used and, finally, M_A undergoes changes according to the variation of lengths of the cameras aluminum structure (α_{Al}). Applying all these changes, (5) becomes

$$\alpha_R = \frac{D_0 * (1 + \alpha_{Al}\Delta T + \alpha_{\text{Steel}} . \Delta T - \alpha_{Si} . \Delta T)}{2 * S'_0 * M_{A_0}}. \tag{7}$$

III. Uncertainty

According to the JCGM 100 : GUM [11], the combined uncertainty $u_c^2(y)$ is given by

$$u_c^2(y) = \sum_{i=1}^{N} \left(\frac{\partial f}{\partial x_i}\right)^2 u^2(x_i) + 2\sum_{i=1}^{N-1}\sum_{j=i+1}^{N} \frac{\partial f}{\partial x_i}\frac{\partial f}{\partial x_j} u(x_i, x_j)$$

$$= \sum_{i=1}^{N} (c_i)^2 u^2(x_i) + 2\sum_{i=1}^{N-1}\sum_{j=i+1}^{N} c_i c_j u(x_i) u(x_j) r_{ij}. \tag{8}$$

This means that the measurement is related to N magnitudes x_i (input quantities), with $i = 1, 2, \ldots, N$, through the functional relation $y = f(x_1, x_2, \ldots, x_N)$. c_i and c_j are the sensitivity coefficients: they indicate the weight of each uncertainty $u(x_i)$. On the other hand, r_{ij} is the estimated correlation coefficient between x_i and x_j. If they are independent, $r_{ij} = 0$. In this paper, we consider the worst case: all the input estimates are correlated with $r_{ij} = \pm 1$.

In order to apply (8), it is necessary to calculate each of the contributions to the uncertainty that appears in A&I. In our case, the value α_R measured by A&I has a specific uncertainty produced by the following quantities x_i:

$$\alpha_R = f(D_0, S'_0, M_{A_0}, \Delta T_{Al}, \Delta T_{\text{Steel}}, \Delta T_{Si}, \alpha_{Al}, \alpha_{\text{Steel}}, \alpha_{Si}).$$

On the other hand, each of the input quantities has its own uncertainty $u(x_i)$. They have to be measured directly or simply estimated.

The measurement performed for our method found that D_0, S'_0, and M_{A_0} have their respective contribution u_V [V as defined in (6)] to the $u(\alpha_R)$ (uncertainty in the angle measurement). Each u_V is the combination of the following set of uncertainties.

1) u_0 = temperature.
2) u_1 = detection software + noise + camera focus.
3) u_2 = Savitzky–Golay filter (vignetting effect).
4) u_3 = pixels position on the CCD.
5) u_4 = light source + power supply.
6) u_5 = pixels matrix orientation with respect to the cross.
7) u_6 = scale's linearity + autocollimator's optics + camera's optics + optical axis alignment.
8) u_7 = beam parallelism + mirror flatness + autocollimator's optics.
9) u_8 = air turbulence.

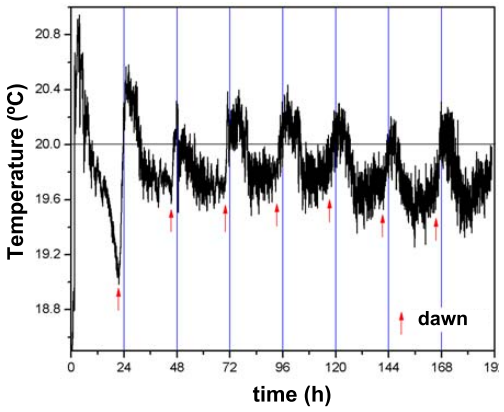

Fig. 5. Temperature behavior at the CEMETRO Laboratory.

The temperature uncertainty affects all input quantities; their contribution will be taken into account in (8). On the other hand, the uncertainties u_1 to u_5 are the contributions to u_D; u_6 is the contribution to $u_{S'}$; and finally, u_7 and u_8 are those related to $M_A(u_{M_A})$. Then, each one is studied and calculated.

It is worth clarifying that we use the notation $u_{x_i} = c_{x_i} . u(x_i)$ in such a way that u_{x_i} represents the contribution of x_i to $u_c^2(y)$. This notation is consistent with [11, Sec. V].

A. Temperature

The CEMETRO Laboratory has an acclimation system that maintains the thermal stability at 20 ± 0.5 °C. Its behavior oscillates, as shown in Fig. 5.

In the worst case, there is a temperature gradient in relation to time determined by

$$G_{T_{\text{MAX}}} = \frac{0.05\ ^\circ\text{C}}{\text{min}}. \tag{9}$$

The maximum temperature variation in 5 min of measurement (the amount of time needed to perform a conventional measurement), according to (9) is $\Delta T = 0.25$ °C. On the other hand, if we suppose a rectangular distribution around the mean value of $\Delta T = 0.5$ °C, we can approximate $u(\Delta T)$ as: $u(\Delta T) = \Delta T/\sqrt{3} \sim 0.3$ °C. Based on these values, we take the following reference value: $u(\Delta T) = 0.3$ °C.

B. Detection Software + Noise + Camera Focus

The uncertainties studied according to the Gaussian detector indicate that the smallest angle the software can obtain is 0.012 arc seconds [7]. In other words, the software's mean squared deviation for each measurement is $s = 0.012''$.

Since the images are averaged N times ($N = 20$), the uncertainty is reduced by that factor [1]

$$u_1 = \frac{s}{\sqrt{N}} = 0.0027''. \tag{10}$$

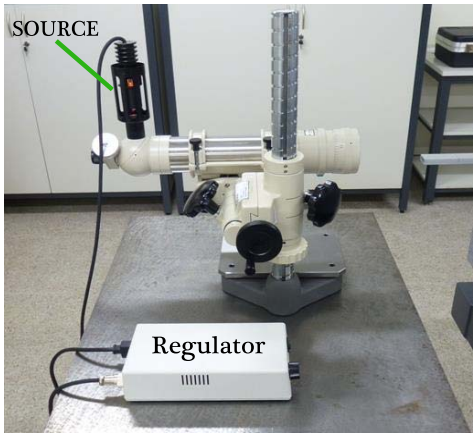

Fig. 6. Nikon autocollimator (beam generating lamp and its regulator are highlighted).

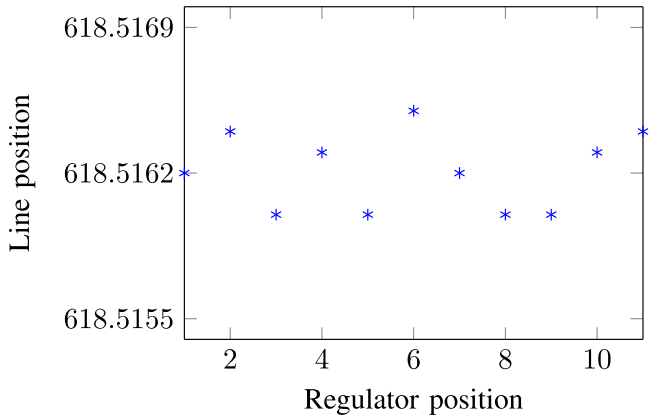

Fig. 7. Positions obtained from the cross horizontal line as the light intensity source is changed.

C. Savitzky–Golay Filter (Vignetting Effect)

Using the following equation:

$$\Delta_B = s_B * \sigma^2 \tag{11}$$

which corresponds to the centroid shift (Δ_B) caused by the effects of vignetting, we can estimate u_2 in arc second as

$$u_2 = \frac{2 * \Delta_B}{97.31 * 7} = 0.001''. \tag{12}$$

The factor 7 is introduced on the basis that the shift affects simultaneously the eight segments when the scale is segmented in our image processing technique [7].

D. Pixels Position on the CCD

The pixel array has small irregularities, which are inherent of the construction method. These result in a disparate position of the pixels in the sensor. In [12], this drift was studied through a measurement procedure performed with a comparator. In this paper, we took regulated measurement steps that determined the irregularities in the pixel lines, concluding that uncertainties similar to the $0.002''$ are introduced. This value is taken as representative

$$u_3 = 0.002''. \tag{13}$$

E. Light Source + Power Supply

The Nikon autocollimator has an adjustable light source responsible for generating the light beam of the cross. The uncertainty associated with the variation of this beam in regard to intensity was studied. In Fig. 6, we can distinguish both the lamp (light source) and its regulator. The latter can form 11 different cross widths.

The cross position was measured for each of the 11 widths of the regulator and a linear model was created to ascertain the mean squared dispersion as a representative value of the uncertainty. The resulting data are shown in Fig. 7. The calculated uncertainty was

$$u_4 = 0.0001''. \tag{14}$$

It should be noted that the power line does not introduce changes in the captures made with the CCD camera.

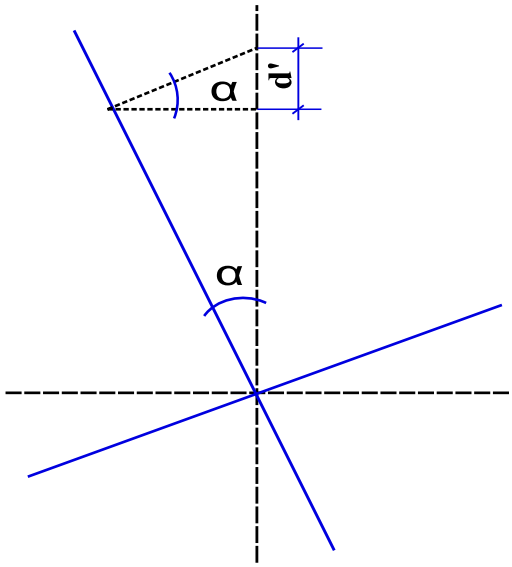

Fig. 8. Final alignment of the cross with an offset of two pixels that produces an angle of inclination α.

The camera's power supply works steadily with 12 VDC ($\pm 10\%$) and a ripple $<1\%$. Within these ranges, the images are not distorted because the data generated in the ADC have the quality described in the data sheet provided by the manufacturer.

F. Pixels Matrix Orientation With Respect to the Cross

Reference [6] explains the procedure for aligning the cross with respect to the pixels of the CCD. In addition, in [7], a study about the lines' detection quality with the image processing as they are tilted is presented. The line tilts two pixels maximum due to residual misalignment and introduces an uncertainty. In Fig. 8, this uncertainty is detailed: the cross with dashed lines corresponds to the ideal position, whereas the inclined cross, in a continuous line, has a slope α produced by the two pixels misalignment. This inclination produces d' difference in the autocollimator's measurement. Through the corresponding calculation for a full-scale measurement, we obtain

$$u_5 = 0.0006''. \tag{15}$$

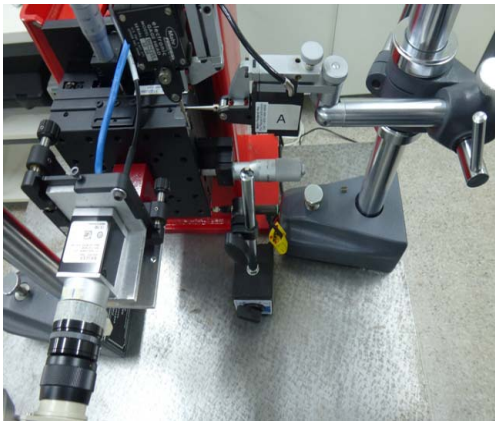

(a)

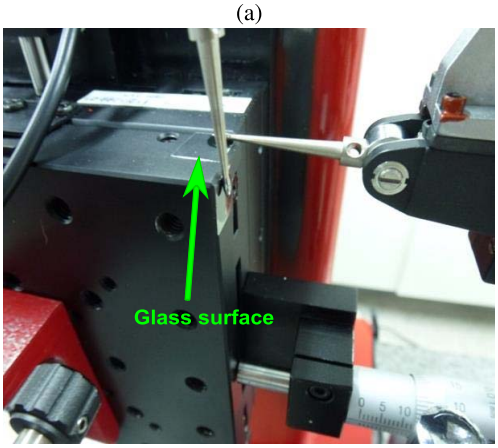

(b)

Fig. 9. Experimental setup for determining the optical system's distortion. (a) Global view of the experiment. (b) View of Mahr Federal gauge heads.

G. Scale's Linearity + Autocollimator's Optics + Camera's Optics + Optical Axis Alignment

In our last conference paper (I2MTC 2017) [8], we describe this uncertainty in detail. In the following, we present only the experiment setup and the calculated uncertainty: the experiment mounted for this analysis can be seen in Fig. 9. We measured the displacement of the plane (σ_x, σ_y) of the camera with a set of three high-resolution electronic gauge heads Mahr Federal LVDT. These gauge heads can measure in a range of ± 0.250 mm with a resolution of 0.1 μm. The pixel size of our camera is 4.4 μm; thus, these gauge heads can measure displacements at subpixel level (1/44 of a pixel). As the resolution of these instruments is very high, they were supported on glass surfaces with a roughness less than 10 nm.

The translational system was moved within a maximum range of ± 0.15 mm, both vertically and horizontally, forming a mechanical capturing grid for the camera. The regular steps were generated by holding the camera in focus and ensuring that its visual field did not capture the edge of the autocollimator's eyepiece (this generates unwanted shadows on the images). An array of captures was created. It was made up of 120 points corresponding to 120 scale images. All these images were processed with a subpixel detection algorithm explained in [5] and [7].

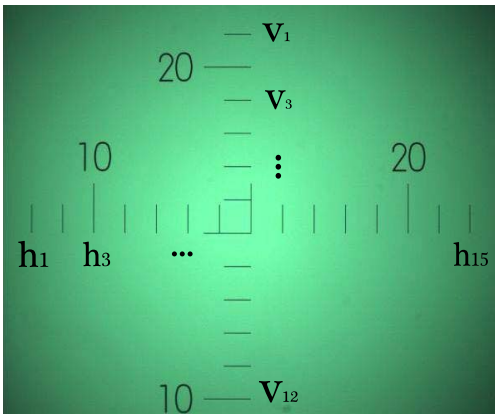

Fig. 10. Virtual scale segments analyzed: 12 vertical and 15 horizontal segments. The image of these segments is on the CCD plane (X, Y).

The segments $(h_1, h_2, \ldots, h_{15})$ and $(v_1, v_2, \ldots, v_{12})$ shown in Fig. 10 are captured and detected. Then, the scale's straight segment shifts were measured to find the distortion based on these captures. Their subpixel shifts are measured as the optical axis of the camera moves relative to the instrument's optical axis.

The uncertainty of the optical assembly when there is a misalignment is an additional datum that emerges from our method. It is worth mentioning that it is also necessary to include an angular dependence because the misalignment contribution is strongly asymmetric [13]. In this paper, however, this dependence was not included because only one direction is discussed.

If a calibration is performed in one direction and the values found want be used for the perpendicular direction, a contribution should be added to the uncertainty of the scale. The contribution is

$$u_6 = 0.06'' \tag{16}$$

for the central region $(\pm 30'')$ and up to $u_6 = 1.7''$ if the whole scale $(\pm 900'')$ is used.

H. Beam Parallelism + Mirror Flatness + Autocollimator's Optics

The flatness of the polished mirror (schematized as E in Fig. 2) is not perfect and affects the image of the cross, making it appears as out of focus. This is due to the optical parallax that produces no coincidence between the plane of the cross and the objective's focal plane. To correct this uncertainty, the autocollimator has a parallax compensating device in its optical system (the device varies according to the model).

The following method should be applied: the scale's compensator ring is positioned in division number 100 and then it is moved from there in a range of ± 0.5 divisions until the beam is in focus. With this correction, the uncertainty u_7 rounds the software uncertainty value $(u_7 = 0.0025'')$.

I. Air Turbulence

The uncertainty introduced by air turbulence was measured. A sequence of images of the cross was captured

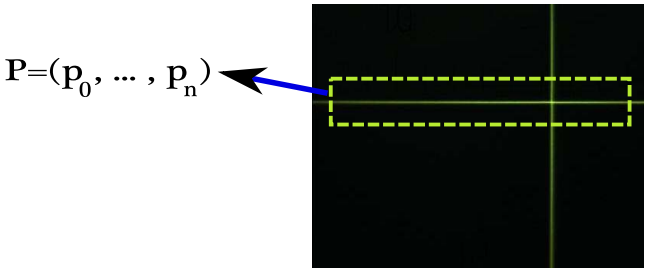

Fig. 11. Detection of the cross horizontal positions to study the behavior of uncertainty according to air turbulence and reflection in the mirror. n positions are measured over time.

over time. Also, we studied whether the position of the cross changed by the effects of air currents in the laboratory, an issue that usually happens even in the most controlled environments.

The reflecting mirror was fixed at a given angular position and at a distance of 0.5 m from the autocollimator [14]. With this configuration, 50 images were taken, triggering the capture each at $t = 5$ s. Then, the position of the cross was measured with the visual interface and a linear model of the data was created, as in Section III-E. Fig. 11 shows the capture of the horizontal line and its n detected positions. The uncertainty associated with the displacement of the cross due to air turbulence was

$$u_8 = 0.002''. \tag{17}$$

J. Uncertainty of the Thermal Expansion Coefficient

Given the thermal expansion coefficients of the main materials that make up the camera and autocollimator: $\alpha_{\text{Steel}} = 10 \times 10^{-6}1/°\text{C}$, $\alpha_{Al} = 21 \times 10^{-6}1/°\text{C}$, and $\alpha_{Si} = 2 \times 10^{-6}1/°\text{C}$.

An approximation of the uncertainty is calculated, taking into account a rectangular distribution in relation to the mean value of the coefficient. For example, $u(\alpha_{\text{Steel}}) = \alpha_{\text{Steel}}/\sqrt{3} = 5.77 \times 10^{-6}1/°\text{C}$.

IV. Results

A. Standard Uncertainty of D, S′, and M_A

When we have a set of uncertainties associated with an input quantity, these are added in quadrature [11]

$$u_{x_i}^2 = u_1^2 + \cdots + u_n^2. \tag{18}$$

Thus

$$u_D^2 = u_1^2 + u_2^2 + u_3^2 + u_4^2 + u_5^2 = 11.62 \times 10^{-6''} \tag{19}$$

$$u_{S'}^2 = u_6^2 = 0.0036''(\pm 30'') \text{ or } 2.89''(\pm 900'') \tag{20}$$

$$u_{M_A}^2 = u_7^2 + u_8^2 = 0.002''. \tag{21}$$

The values in parenthesis ($\pm 30''$) and ($\pm 900''$) represent the two ranges suggested in [14] that must be analyzed in the autocollimator's field of view.

B. Combined Standard Uncertainty

The final uncertainty calculated is:

$$u_c(\alpha_R) = 0.008''(\pm 30'') \tag{22}$$

$$u_c(\alpha_R) = 4''(\pm 900''). \tag{23}$$

C. Relative Impact of Each Uncertainty Contribution

The remaining action is to find out which part of the instrument A&I has greater influence on uncertainty. In order to achieve this, we calculate the relative impact of each contribution as follows:

$$Ir_{xi} = \frac{u_{x_i}}{u_c(\alpha_R)} \times 100. \tag{24}$$

Through the calculation of both ranges, we obtain $Ir_{S'} = 97.4\%$, $Ir_D = 2.57\%$, and $(Ir_{M_A} + Ir_{\Delta T_{\text{mat}}} + Ir_{\alpha_{\text{mat}}}) = 0.03\%$. As we can observe in Section III-G, the main contribution to $Ir_{S'}$ arises from u_6. Similar values are found by Neale *et al.* [15], in the studio of camera lenses distortion.

V. Discussion in Relation to the State of the Art

Over the last few decades, extensive efforts have been made to achieve reliable angular measurements with optical and electronic autocollimators [16], [17]. The studies that construct the knowledge in this area focus mainly on the calibration stage of the instrument. This is the case of the interesting work by Just *et al.* [12], which presents the calibration of a high-resolution electronic autocollimator against an angle comparator. There is also the excellent work of Brucas and Giniotis [18] that calibrates the autocollimator with a rotary table.

The National Metrology Institute of Germany [Physikalich-Technische Bundesanstalt (PTB)] holds a position of leadership in this segment. One of the main studies performed at PTB with an uncertainty comparator $u = 0.001''$ explains the current status of autocollimators' calibrations [19].

All these studies focus on the final stage of the instrument's calibration, which, in terms of uncertainty, is called "uncertainty of the angular patterns." In our method, we did not include it, since this paper focused on the detailed study of all the other contributions that appear when assembling the camera in the autocollimator. At this stage of design, it is important to find out where the main sources of error are and then minimize them. These contributions are not calculated in the other studies and must be identified before the final calibration step.

VI. Conclusion and Future Work

This development presents the analysis of uncertainty due to the contributions that appear in the measurement with the new instrument A&I. The contributions are derived from the input quantities x_i obtained from the mathematical model of A&I.

The study of uncertainty clearly expresses that the errors by misalignment introduced by the camera's optics determine the value of the final uncertainty $u_c(\alpha_R)$. Its relative impact on $u_c(\alpha_R)$ is 97.4%. If the quality of the lens is improved, the $u_c(\alpha_R)$ will decrease noticeably. The camera lens, which currently presents a 3% of distortion, must be replaced by a lens with 0.1% of distortion. Replacing the original lens with a 0.1% lens will allow the movement from $4''$ to $0.1''$ alignment over the entire range of the scale (an amount that is in accordance with the measurements using digital autocollimators).

It should be noted that the constructed mathematical model can be applied in a similar way for other optical autocollimators to which a low-cost visual interface is added. With the model and the procedures developed in this paper, other laboratories can design interfaces that enable the improvement of their instruments' BMC.

The last step is a final stage in the design of A&I: an accurate calibration including the uncertainty of the patterns. In a calibration process, the measured values are D associated with each angle α (generated with a highly accurate traceable instrument). Thus, this value $c = \alpha/D = 1/(2 \,.\, S' \,.\, M_A)$ is obtained. This procedure is useful to correct alignments with greater accuracy, as long as the new optics for the camera is available, and the system is mounted in conjunction with the autocollimator using a high-quality mechanical part. In this stage, it is necessary to work with a bar which generates the high accuracy angles, at least five times smaller than the final uncertainty ($u_{\text{bar}} = 0.001''$). This bar should move in known regular steps. In this case, the bar would be the reference instrument, replacing the electronic level already used in our previous work.

ACKNOWLEDGMENT

This development was made possible by CEMETRO metrology center's equipment.

REFERENCES

[1] J. Taylor, *Introduction To Error Analysis: The Study of Uncertainties in Physical Measurements*. South Orange, NJ, USA: Univ. Science Books, 1997.

[2] W. T. Estler, "Uncertainty analysis for angle calibrations using circle closure," *J. Res. Nat. Inst. Standards Technol.*, vol. 103, no. 2, pp. 141–151, 1998.

[3] *C of Investigation and T in Metrology (CEMETRO)*. [Online]. Available: http://www.investigacion.frc.utn.edu.ar/cemetro/laboratorio.html

[4] C. Schurrer, A. G. Flesia, G. Bergues, G. Ames, and L. Canali, "Interfaz visual para un autocolimador nikon 6d mediante procesamiento de imágenes con precisión sub-píxel: Un caso de estudio," *Rev. Iberoamericana Autom. Inf. Ind.*, vol. 11, no. 3, pp. 327–336, 2014.

[5] A. G. Flesia, G. Ames, G. Bergues, L. Canali, and C. Schurrer, "Subpixel straight lines detection for measuring through machine vision," in *Proc. IEEE Instrum. Meas. Technol. Conf. (I2MTC)*, May 2014, pp. 402–406.

[6] G. Bergues, G. Ames, L. Canali, C. Schurrer, and A. G. Flesia, "External visual interface for a nikon 6d autocollimator," in *Proc. IEEE Int. Instrum. Meas. Technol. Conf. (I2MTC)*, May 2014, pp. 35–39.

[7] G. J. Bergues, L. Canali, C. Schurrer, and A. G. Flesia, "Electronic interface with vignetting effect reduction for a Nikon 6B/6D autocollimator," *IEEE Trans. Instrum. Meas.*, vol. 64, no. 12, pp. 3500–3509, Dec. 2015.

[8] G. Bergues, C. Schurrer, N. Brambilla, and L. Canali, "Misalignment contribution to the autocollimator's scale distortion," in *Proc. IEEE Int. Instrum. Meas. Technol. Conf. (I2MTC)*, May 2017, pp. 1–5.

[9] K. Hume, *Metrology With Autocollimators*. London, U.K.: Hilger & Watts, 1965.

[10] E. Hecht, *Optics*, 4th ed. Reading, MA, USA: Addison-Wesley, Aug. 2001.

[11] "JCGM 100: Evaluation of measurement data—Guide to the expression of uncertainty in measurement," JCGM, Tech. Rep., 2008.

[12] A. Just, M. Krause, R. Probst, and R. Wittekopf, "Calibration of high-resolution electronic autocollimators against an angle comparator," *Metrologia*, vol. 40, no. 5, p. 288, 2003.

[13] K. Thompson, "Aberration field in tilted and decentered optical systems," Ph.D. dissertation, Univ. Arizona, Tucson, AZ, USA, 1980.

[14] R. D. Geckeler and A. Just, "Supplementary comparison euramet.l-k3a.2009 angle comparison using an autocollimator," Eur. Assoc. Nat. Metrol. Inst., Tech. Rep., 2009.

[15] W. Neale, D. Hessel, and T. Terpstra, "Photogrammetric measurement error associated with lens distortion," SAE Tech. Paper 2011-01-0286, 2011.

[16] S. G. Alcock *et al.*, "The diamond-nom: A non-contact profiler capable of characterizing optical figure error with sub-nanometre repeatability," *Nucl. Instrum. Methods Phys. Res. A, Accel. Spectrom. Detect. Assoc. Equip.*, vol. 616, nos. 2–3, pp. 224–228, 2010.

[17] J. Yuan and X. Long, "CCD-area-based autocollimator for precision small-angle measurement," *Rev. Sci. Instrum.*, vol. 74, no. 3, pp. 1362–1365, 2003.

[18] D. Brucas and V. Giniotis, "Calibration of precision polygon/autocollimator measurement system," *J. Phys., Conf. Ser.*, vol. 238, no. 1, p. 012014, 2010.

[19] R. Geckeler, A. Just, M. Krause, and H. Bosse, "Autocollimator characterization and calibration at the PTB: Current status and future progress," in *Proc. 10th Int. Symp. Meas. Quality Control (ISMQC)*, 2010, pp. 55–58.

Guillermo J. Bergues was born in Buenos Aires, Argentina, in 1984. He received the Degree in electronic engineering and the Ph.D. degree from Universidad Tecnológica Nacional, Córdoba, Argentina, in 2010 and 2015, respectively.

He is currently a Metrologist with the Centro de Investigación y Transferencia en Metrología Laboratory, Córdoba, where he carries out his research. His current research interests include language for machine vision and image processing techniques for metrological applications.

Clemar Schürrer received the Ph.D. degree in physics from the Faculty of Mathematics, Astronomy and Physics, National University of Córdoba, Córdoba, Argentina, in 1995.

His current research interests include angle metrology applied to surface characterization forms.

Nancy Brambilla received the Degree in electric electronic engineering and the M.Sc. degree from the National University of Córdoba (UNC), Córdoba, Argentina, in 1990 and 2014, respectively.

She is currently a Professor with the Basic Sciences Department, Universidad Tecnológica Nacional (UTN), Córdoba, where she is the Chairman of the Centro de Investigación y Transferencia en Metrología. She is the Chairman of the UTN Post-Graduate Program and a Quality Engineer and a Professor with the Electronic Department of Engineer Branch, UNC. Her current research interests include metrology, uncertainty, quality control, and signal processing.